Supplementary information for

Electrolyte effects on the stability and CO binding of copper chloride complexes for electrochemical separation of CO/N_2

Authors: Christel I. Koopman[1,2], Jelco Albertsma[1], Zhengyao Zhu[1,2], Monique A. van der Veen[1], David A. Vermaas[1,2]

[1] Department of Chemical Engineering, Delft University of Technology, Van der Maasweg 9, 2629HZ, Delft, Netherlands

[2] e-Refinery Institute, Leeghwaterstraat 39, 2628CB, Delft, the Netherlands

Contents

SI-1 Binding constant to selectivity and capacity utilisation

The binding constant can be used to find a theoretical upper limit to the selectivity and capacity utilisation. For a system where Cu^+ is the carrier and CO is the ligand Equation S1, S2 and S3 describe the relation for the binding constant (K_{CO}), the dissolved CO concentration and the total Cu^+ concentration. Binding of a single CO to Cu^+ is assumed.

$$K_{CO} = \frac{[Cu^+CO]}{[Cu^+][CO]} \tag{S1}$$

$$[CO] = H_{CO} \cdot P_{CO} \tag{S2}$$

$$[Cu^+]_{tot} = [Cu^+] + [Cu^+CO] \tag{S3}$$

Here, H_{CO} is the Henry constant for CO in water (0.00095 M bar^{-1}), P_{CO} is the partial pressure of CO (bar) and [X] represents the concentration of X (M). Combining the three equations gives an expression for the Cu^+CO concentration (Equation S4).

$$[Cu^+CO] = \frac{K_{CO}\cdot[Cu^+]_{tot}\cdot H_{CO}\cdot P_{CO}}{1+K_{CO}\cdot H_{CO}\cdot P_{CO}} \tag{S4}$$

The capacity utilisation is expressed as the fraction of carrier that actually carries a CO (Equation S5).

$$Capacity\ utilisation = \frac{[Cu^+CO]}{[Cu^+]_{tot}} = \frac{K_{CO}\cdot H_{CO}\cdot P_{CO}}{1+K_{CO}\cdot H_{CO}\cdot P_{CO}} \tag{S5}$$

The sorbent solution with activated carrier has the following solubility of CO and N_2:

$$[CO]_{tot} = H_{CO} \cdot P_{CO} + \frac{K_{CO}\cdot[Cu^+]_{tot}\cdot H_{CO}\cdot P_{CO}}{1+K_{CO}\cdot H_{CO}\cdot P_{CO}} \tag{S6}$$

$$[N_2]_{tot} = H_{N_2} \cdot P_{N_2} \tag{S7}$$

The N_2 concentration is from N_2 dissolution in the solvent following Henry's law, while the CO concentration is both the dissolution and the chemical absorption to the carrier. The uptake ratio is the ratio of the total CO concentration over the total N_2 concentration (Equation S8) and is presented as a function of K_{CO} in Figure S1 at different CO partial pressures.

$$Uptake\ ratio = \frac{[CO]_{tot}}{[N_2]_{tot}} = \frac{H_{CO}\cdot P_{CO}}{H_{N_2}\cdot P_{N_2}}\left(1 + \frac{K_{CO}\cdot[Cu^+]_{tot}}{1+K_{CO}\cdot H_{CO}\cdot P_{CO}}\right) \tag{S8}$$

The solution's affinity or selectivity (α) can be expressed as the normalized ratio of the effective solubilities:[1]

$$\alpha = \frac{[CO]_{tot}/P_{CO}}{[N_2]_{tot}/P_{N_2}} = \frac{H_{CO}}{H_{N_2}}\left(1 + \frac{K_{CO}\cdot[Cu^+]_{tot}}{1+K_{CO}\cdot H_{CO}\cdot P_{CO}}\right) \tag{S9}$$

The solution's selectivity is the ratio of the Henry's constants with an additional term from the added CO solubility introduced by the carrier. This term includes the binding constant, total carrier concentration and the partial pressure of CO. With increasing partial pressure of CO this term becomes less important for the selectivity due to saturation of the carrier. Thus the selectivity will decrease to ratio of the Henry constants while the uptake ratio increases due to higher dissolution of CO compared to N_2.

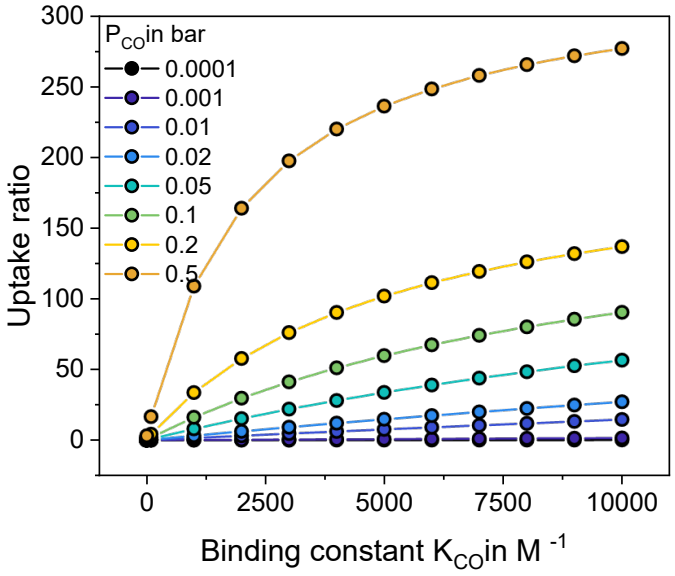

Figure S1: Uptake ratio defined as the total amount of CO dissolved divided by the total amount of N_2 dissolved inside the activated carrier solution with a carrier concentration of 0.1M and an assumed total pressure of 1 bar.

SI-2 Derivation of effect of CO equilibrium on Nernst equation

Starting from the Nernst equation for Cu^+ and Cu^{2+} and the CO-carrier equilibrium constant (Equation S10, S11 and S12).

$$E = E^{0\prime} + \frac{RT}{nF}\ln\left(\frac{[\mathrm{Cu}^{2+}]}{[\mathrm{Cu}^{+}]}\right) \tag{S10}$$

$$K_{CO}^{I} = \frac{[Cu^{+}CO]}{[Cu^{+}][CO]} \tag{S11}$$

$$K_{CO}^{II} = \frac{[Cu^{2+}CO]}{[Cu^{2+}][CO]} \tag{S12}$$

Here, E is the equilibrium potential (V vs ref), R is the gas constant (8.3145 J mol^{-1} K^{-1}), T is temperature (K), n is the number of electrons, F is the Faraday constant (96485 C mol^{-1}), [X] is the concentration of X, and K_{CO}^{I} and K_{CO}^{II} are the binding constants between CO and Cu^+ or Cu^{2+} respectively (M^{-1}).

These binding constants between CO and Cu^+ (K_{CO}^{I}) and CO and Cu^{2+} (K_{CO}^{II}) will affect the concentration ratio term in the Nernst equation, as the total concentration of Cu^+ species and Cu^{2+} species in solution is described by:

$$[\mathrm{Cu}^{+}]_{tot} = [\mathrm{Cu}^{+}] + [\mathrm{Cu}^{+}\mathrm{CO}] = [\mathrm{Cu}^{+}] + K_{CO}^{I} \cdot [CO] \cdot [\mathrm{Cu}^{+}] \tag{S13}$$

$$[\mathrm{Cu}^{2+}]_{tot} = [\mathrm{Cu}^{2+}] + [\mathrm{Cu}^{2+}\mathrm{CO}] = [\mathrm{Cu}^{2+}] + K_{CO}^{II} \cdot [CO] \cdot [\mathrm{Cu}^{2+}] \tag{S14}$$

Rewriting Equation S13 and S14 to expressions of $[Cu^+]$ and $[Cu^{2+}]$ and substituting them in the Nernst equation gives an expression for the Nernst equation of the Cu^+/Cu^{2+} redox couple in the presence of CO.

$$E^{CO} = E^{0\prime} + \frac{RT}{nF}\ln\left(\frac{1+K_{CO}^{I}\cdot[CO]}{1+K_{CO}^{II}\cdot[CO]}\right) + \frac{RT}{nF}\ln\left(\frac{[\mathrm{Cu}^{2+}]_{tot}}{[\mathrm{Cu}^{+}]_{tot}}\right) \quad \text{(S15)}$$

Subtracting the equilibrium potential under N_2 (Equation S10) from the equilibrium potential under CO (Equation S15) shows the expected shift of potential with CO concentration as a function of the CO binding constants (Equation S16).

$$\Delta E = E^{CO} - E^{N_2} = \frac{RT}{nF}\ln\left(\frac{1+K_{CO}^{I}\cdot[CO]}{1+K_{CO}^{II}\cdot[CO]}\right) \quad \text{(S16)}$$

Derivation from Gibbs free energy

When a system is at equilibrium (KG = 0), the standard Gibbs free energy change (ΔG^0) describes the equilibrium constant (K).

$$\Delta G = \Delta G^0 + RTln(Q) \quad \text{(S17)}$$

$$\Delta G^0 = -RTln(K) \quad \text{(S18)}$$

Here, Q is the reaction quotient of a chemical equilibrium reaction. These equations are also the basis for the Nernst equation as the Gibbs free energy is related to the potential (E).

$$\Delta G = -nFE \quad \text{(S19)}$$

Combining Equation S17 with S19 gives the Nernst equation:

$$E = E^{0\prime} + \frac{RT}{nF}\ln(Q) \quad \text{(S20)}$$

When we look at the redox reaction of Cu^{2+}/Cu^{+} and the equilibrium reactions between CO and Cu^{2+} and Cu^{+} we can express the effect of CO binding on the equilibrium potential.

$$Cu^{2+} + e^{-} \leftrightarrow Cu^{+} \quad \text{rxn1}$$

$$Cu^{2+} + CO \overset{K_{CO}^{II}}{\longleftrightarrow} Cu^{2+}CO \quad \text{rxn2}$$

$$Cu^{+} + CO \overset{K_{CO}^{I}}{\longleftrightarrow} Cu^{+}CO \quad \text{rxn3}$$

$$Cu^{2+}CO + e^{-} \leftrightarrow Cu^{+}CO \quad \text{rxn4}$$

Reaction 1 and 4 are the electrochemical equilibrium reactions between Cu^{+} and Cu^{2+} with and without CO coordination. Reaction 2 and 3 describe the equilibrium between CO and Cu^{2+} and Cu^{+}, respectively. If the binding of CO is favoured for one of the oxidation states, it will pull the equilibrium towards that side of the reaction, which will be represented in the equilibrium potential (Figure S2). Reaction 4 can be obtained by combining reaction 1, 2 and 3:

$$\Delta G_4^0 = \Delta G_1^0 - \Delta G_2^0 + \Delta G_3^0 \quad \text{(S21)}$$

Substituting Equation S18 into S21 for the CO equilibria gives:

$$\Delta G_4^0 = \Delta G_1^0 + RTln(K_{CO}^{II}) - RTln(K_{CO}^{I}) = \Delta G_1^0 + RTln\left(\frac{K_{CO}^{II}}{K_{CO}^{I}}\right) \quad \text{(S22)}$$

Now using Equation S19 to describe the standard Gibbs free energy changes as standard reduction potentials gives:

$$E_4^0 = E_1^0 + \frac{RT}{nF} ln\left(\frac{K_{CO}^I}{K_{CO}^{II}}\right) \quad \text{(S23)}$$

This expresses the change in the standard redox potential of the Cu^{2+}/Cu^{+} redox by the binding of CO. This can also be obtained by starting from the Nernst equations and the expression of the binding constant.

$$E_{Cu^{2+}/Cu^{+}} = E^{0\prime}_{Cu^{2+}/Cu^{+}} + \frac{RT}{nF}\ln\left(\frac{[\mathrm{Cu}^{2+}]}{[\mathrm{Cu}^{+}]}\right) \quad \text{(S24)}$$

$$E_{Cu^{2+}CO/Cu^{+}CO} = E^{0\prime}_{Cu^{2+}CO/Cu^{+}CO} + \frac{RT}{nF}\ln\left(\frac{[\mathrm{Cu}^{2+}CO]}{[\mathrm{Cu}^{+}CO]}\right) \quad \text{(S25)}$$

$$K_{CO}^I = \frac{[Cu^{+}{-}CO]}{[Cu^{+}][CO]} \quad \text{(S26)}$$

$$K_{CO}^{II} = \frac{[Cu^{2+}{-}CO]}{[Cu^{2+}][CO]} \quad \text{(S27)}$$

Rewriting S26 and S27 to get an expression for $[Cu^{2+}]$ and $[Cu^{+}]$ and substituting this in Equation S24 gives a Nernst equation for the CO-bound $Cu^{2+}CO/Cu^{+}CO$:

$$E_{Cu^{2+}CO/Cu^{+}CO} = E^{0\prime}_{Cu^{2+}/Cu^{+}} + \frac{RT}{nF}\ln\left(\frac{\frac{[\mathrm{Cu}^{2+}CO]}{K_{CO}^{II}[CO]}}{\frac{[\mathrm{Cu}^{+}CO]}{K_{CO}^{I}[CO]}}\right) = E^{0\prime}_{Cu^{2+}/Cu^{+}} + \frac{RT}{nF} ln\left(\frac{K_{CO}^I}{K_{CO}^{II}}\right) + \frac{RT}{nF}\ln\left(\frac{[\mathrm{Cu}^{2+}CO]}{[\mathrm{Cu}^{+}CO]}\right) \quad \text{(S28)}$$

If the Nernst Equation of the CO-bound $Cu^{2+}CO/Cu^{+}CO$ is described by Equation S25, then this gives the same relation between the standard potentials as described in S23:

$$E^{0\prime}_{Cu^{2+}CO/Cu^{+}CO} = E^{0\prime}_{Cu^{2+}/Cu^{+}} + \frac{RT}{nF} ln\left(\frac{K_{CO}^I}{K_{CO}^{II}}\right) \quad \text{(S29)}$$

Both expression S24 and S28 can be rewritten to obtain an expression of the shift in potential as a function of CO concentration as shown in the main text by introducing the total concentration of Cu^{+} and Cu^{2+}.

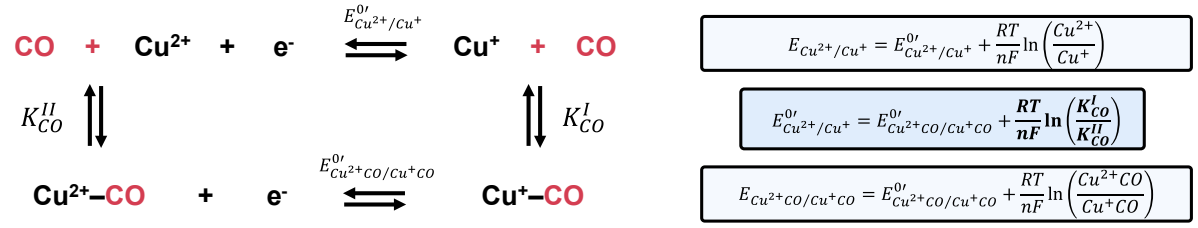

Figure S2: Binding of CO to Cu^{+} and/or Cu^{2+} will shift the Nernst equilibrium of the redox couple and depends on the binding constants (K_{CO}^I and K_{CO}^{II}).

SI-3 Data processing CV measurements

The relation between the shift in potential and the CO concentration can be used to estimate the binding constant between the carrier and CO. [2-5]

$$\Delta E = \frac{RT}{nF} \ln\left(1 + K_{CO} \cdot [CO]\right) \quad \text{(S30)}$$

Here ΔE is the shift in potential (V), R is the gas constant (8.3145 J mol^{-1} K^{-1}), T is the temperature (K), n is the number of electrons, F is the Faraday constant (94658 C mol^{-1}) and K_{CO} is the binding constant between CO and Cu^{+} in our case, assuming a single terminal CO ligand. The equation can be expressed in a form that allows us to obtain the binding constant from the slope of a linear curve.

$$K_{CO} \cdot H_{CO} \cdot P_{CO} = exp\left(\frac{nF}{RT}\Delta E\right) - 1 \quad \text{(S31)}$$

Plotting the exp($nf\Delta E$)-1 against the partial pressure (P_{CO}) should result in a linear line with slope being the product of the binding constant and Henry constant (H_{CO}). Equation S31 describes the shift in potential compared to the potential in the absence of CO. However, the first CO step (5 vol%) would typically show a disproportionate shift compared to the other points. This could potentially be caused by shifting of the reference electrode in the presence of CO. Therefore, Equation S31 was rewritten to omit the 0 CO data point for the estimation of K_{CO}.

$$K_{CO} \cdot H_{CO} \cdot P_{CO,i} + 1 = exp\left(\frac{nF}{RT}\left(E_{CO,i} - E_{N_2}\right)\right) \quad \text{(S32)}$$

$$K_{CO} \cdot H_{CO} \cdot P_{CO,j} + 1 = exp\left(\frac{nF}{RT}\left(E_{CO,j} - E_{N_2}\right)\right) \quad \text{(S33)}$$

Equation S32 and S33 is relation S31 at two different partial pressures of CO, $P_{CO,i}$ and $P_{CO,j}$, resulting in different shifts, $E_{CO,i}$ and $E_{CO,j}$, respectively. The two equations can be divided by each other to get an equation that describes the shift between two CO partial pressures.

$$\frac{K_{CO} \cdot H_{CO} \cdot P_{CO,i} + 1}{K_{CO} \cdot H_{CO} \cdot P_{CO,j} + 1} = exp\left(\frac{nF}{RT}\left(E_{CO,i} - E_{CO,j}\right)\right) \quad \text{(S34)}$$

We used the scan at the first CO concentration (5 vol%) as the new base point ($P_{CO,j}$ and $E_{CO,j}$) and calculated the shift against this concentration for the other concentrations (10 – 50 vol%). Plotting the exponent term (right term Equation S34) as a function of the partial pressure of CO gives a linear curve. This can then be fit by a line representing the binding constant term (left term Equation S34). Using data solver in excel, this line can be fit by minimising the mean absolute error between the data points and the K_{CO} fit, resulting in a value for K_{CO} (Figure 3b).

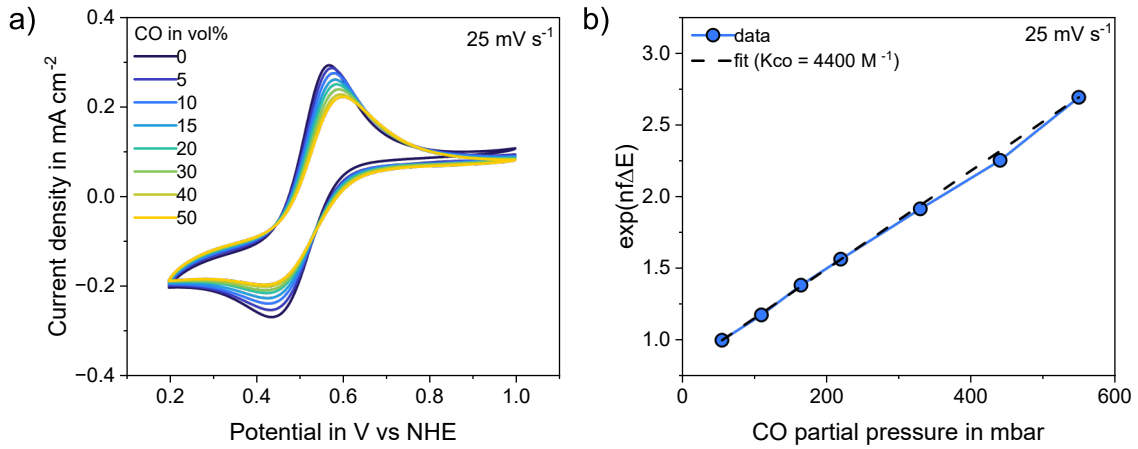

Figure 3: a) Cyclic voltammetry measurement of 2.5 mM CuCl and 2.5mM $CuCl_2$ in 1.25 M $CaCl_2$ 0.03 M HCl electrolyte at 25 mV s^{-1}. The gas flow rate is 2 ml min^{-1} with different CO concentrations and the remaining gas is N_2. b) The shift of the CV measurement plotted against the partial pressure of CO and a fit to minimize the mean average error resulting in a binding constant of 4400 M^{-1}. This figure is Figure 6 in the main text.

Our CV scans shift anodically (to more positive potentials) with CO concentration. However, the shape of the CV scans differ between the electrolyte solutions and some electrolyte solutions have no clear reduction peak (e.g. HCl) (SI-8). As a result, it is impractical to use the half-wave potential to calculate the potential shift. Instead, we used the oxidation peak shift to estimate the binding constant.

The scan rate of the CV measurement needs to be considered with this method. Figure S4 shows the fit of the potential shift in the exponent term with CO concentration at different scan rates.

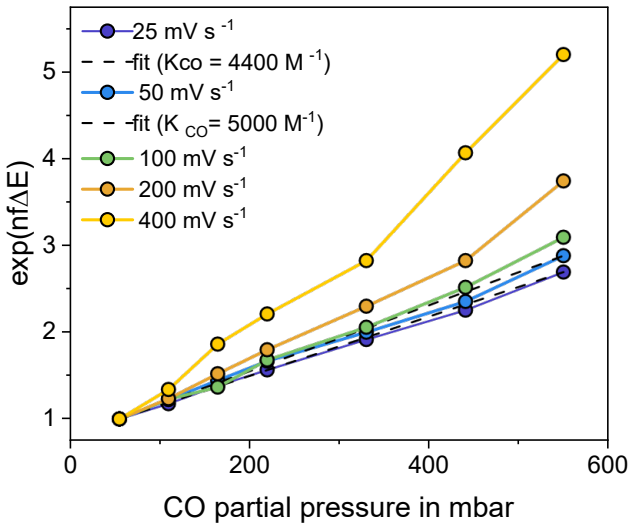

Figure S4: Fit of the potential shift with CO concentration for different CV scan rates for a solution with 2.5 mM CuCl, 2.5 mM $CuCl_2$, 1.25 M $CaCl_2$, and 0.03 M HCl.

With increasing scan rate the shift becomes larger, which cause a steeper slope and this would translate into a larger binding constant. As the CV measurements become less reversible with higher scan rate, we consider the lower scan rates to be more representative. The lower scan rate also provides the system more time to find its equilibrium, both for the redox reaction and the CO coordination. Another consideration with scan rate, is that a slow scan rate will result in more

conversion of Cu to Cu^{+} or Cu^{2+} near the electrode and this will consume more CO. Therefore, the actual CO concentration experienced near the electrode might be lower than expected. An excess of CO is beneficial to this method to maintain a controlled CO concentration. However, due to the low Henry constant for CO in water, this might not be the case in our system, especially at low CO partial pressures.

The coordination of one terminal CO ligand was assumed in the previous derivation and shows a good fit. Other complexes that could be formed are $(Cu^{+})_2CO$ and $Cu^{+}(CO)_2$. This would result in a different relation between the shift, CO concentration and binding constant. Figure S5 shows the fit for each of the possible complexes and shows that $Cu^{+}CO$ is indeed the best fit.

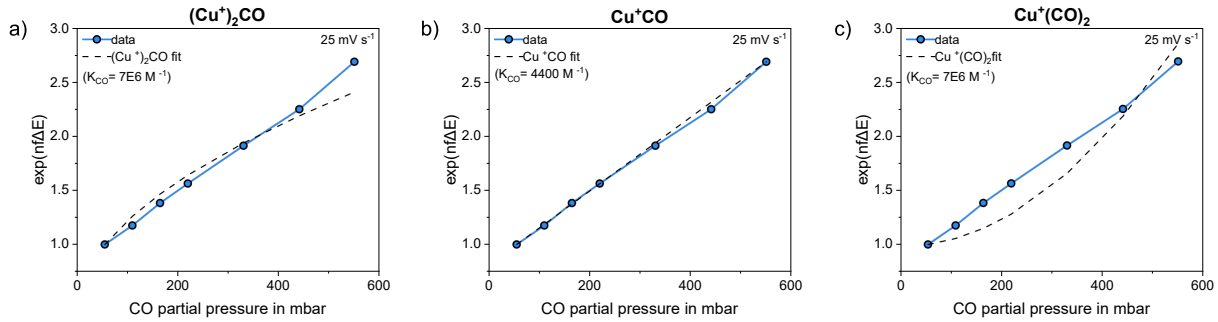

Figure S5: Fit of the potential shift with CO concentration assuming the formation of a) $(Cu^{+})_2CO$, b) $Cu^{+}CO$, and c) $Cu^{+}(CO)_2$. The solution consists of 2.5 mM CuCl, 2.5 mM $CuCl_2$, 1.25 M $CaCl_2$, and 0.03 M HCl.

$(Cu^{+})_2CO$ and $Cu^{+}(CO)_2$ require fitting with Equation S35 and S36, respectively.

$$\frac{K_{CO}\cdot\left(H_{CO}\cdot P_{CO,i}\right)^2+1}{K_{CO}\cdot\left(H_{CO}\cdot P_{CO,j}\right)^2+1} = exp\left(\frac{nF}{RT}\left(E_{CO,i}-E_{CO,j}\right)\right) \quad \text{(S35)}$$

$$\frac{P_{CO,i}}{P_{CO,j}}\cdot\frac{\sqrt{1+8K_{CO}\cdot H_{CO}\cdot P_{CO,j}\cdot[Cu^{+}]_{tot}}-1}{\sqrt{1+8K_{CO}\cdot H_{CO}\cdot P_{CO,i}\cdot[Cu^{+}]_{tot}}-1} = exp\left(\frac{nF}{RT}\left(E_{CO,i}-E_{CO,j}\right)\right) \quad \text{(S36)}$$

Both do not fit the straight line of the data and require very high K_{CO} to be close to the data values (K_{CO} = 7.10^6 M^{-1}). It is not visible in the data if the formation of different carrier-CO complexes happens at slower timescales than the CV measurements.

SI-4 DFT calculations

Orbital analysis (ETS-NOCV) was used to obtain the different orbital energies and distinguish different contributions to the overall binding affinity. Table S1 shows an overview of the Gibbs free energy, enthalpy, orbital energies and CO wavenumber (free CO = 2191.36 cm^{-1}).

Table S1: Changes in energy upon binding of CO obtained from DFT calculation with orbital analysis (ETS-NOCV). The table includes changes in Gibbs free energy (ΔG), enthalpy (ΔH), the complex' total orbital energy ($E_{orbitals}$), sigma-orbital energy (E_{sigma}), pi-orbital energy (E_{pi}) and remaining orbitals energy (E_{rest}) in kJ mol^{-1} and CO wavenumber (ν_{CO}) in cm^{-1}

	$CuCl$ – CO	$CuCl_2^-$ – CO	$CuCl_3^{2-}$ – CO
ΔG (kJ mol^{-1})	-106	-7	-2
ΔH (kJ mol^{-1})	-149	-40	-46
$E_{orbitals}$ (kJ mol^{-1})	-181	-230	-244
E_{sigma} (kJ mol^{-1})	-69	-78	-53
E_{pi} (kJ mol^{-1})	-81	-104	-154
E_{rest} (kJ mol^{-1})	-31	-49	-37
ν_{CO} (cm^{-1})	2201	2108	1998

Although the CO binding becomes less strong with increasing chloride coordination (change in Gibbs free energy becomes less negative), the energy of the complex' orbitals becomes more negative with chloride coordination. Especially the π-orbital's energy shows a decreasing trend with chloride coordination, suggesting that chloride ligands enhance π-backbonding. The stronger π-backbonding with chloride ligands is also reflected in a decreasing CO wavenumber, as pi-backdonation to the antibonding π-orbital should weaken the C-O bond.[6] The decrease in overall binding affinity (Gibbs free energy) is then explained by other factors such as geometrical and electrostatic effects as explained in the main text.

SI-5 Copper chloride solutions

Figure S6 shows pictures of the copper chloride solutions at different chloride concentration for KCl, $CaCl_2$ and HCl. At the lowest chloride concentrations (0.03M HCl), the CuCl and $CuCl_2$ mixture has a light blue colour. With increasing chloride concentration, the solution becomes more green.[7] For KCl, the solution was turbid at 4.0 M and slightly at 2.5 M.

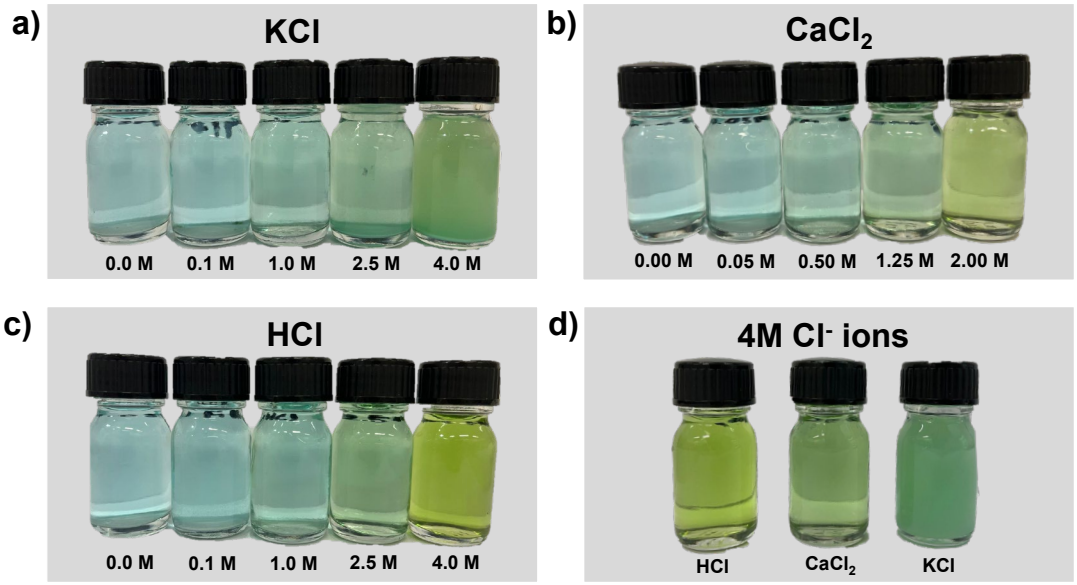

Figure S6: Pictures of copper chloride solutions at different chloride concentrations for a) KCl, b) $CaCl_2$, and c) HCl electrolytes. All solutions contain 0.05 M CuCl, 0.05 M $CuCl_2$ and 0.03 M HCl next to the added electrolytes (KCl, $CaCl_2$ and HCl at the mentioned concentration. d) The solutions at the highest chloride concentration 4 M Cl^- for the different chloride salts.

At the lower chloride concentrations (0, 0.1 and 1.0M) solid deposits were visible at the bottom, most likely due to supersaturation of CuCl at these Cu^+ and Cl^- concentrations (Figure S7).

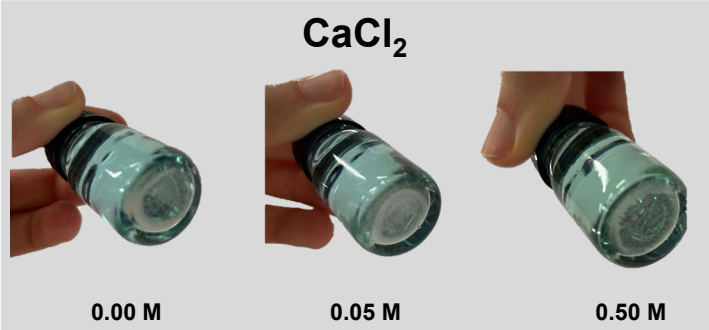

Figure S7: Pictures of the white deposits formed at the lower chloride concentrations. The solutions consist of 0.05 M CuCl, 0.05 M $CuCl_2$, 0.03 M HCl, and the indicated concentration of $CaCl_2$.

SI-6 Composition of copper chloride solutions – Visual Minteq

The composition of different copper chloride solutions was calculated by Visual Minteq. Figure S8 shows the free chloride concentration and chloride activity as a function of total chloride concentration.

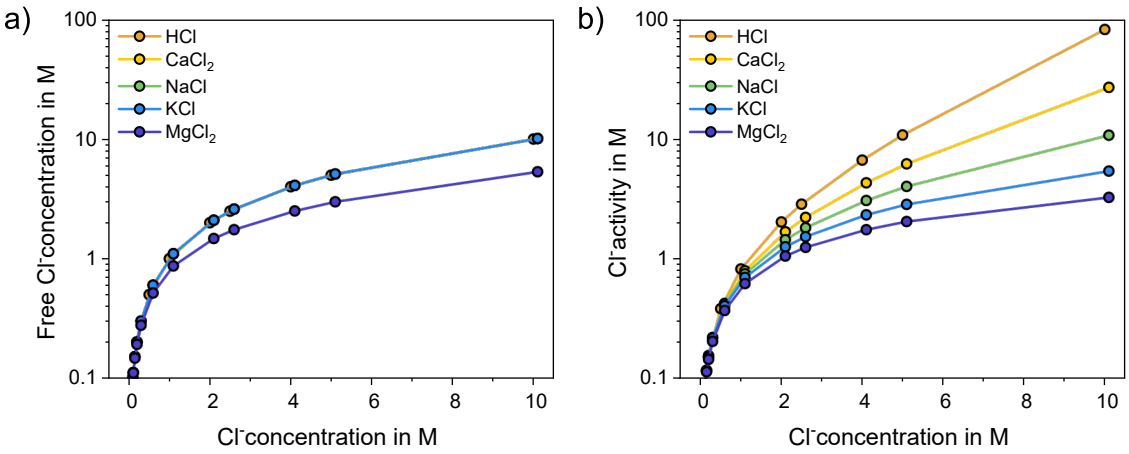

Figure S8: a) Free Cl^- concentration and b) Cl^- activity as a function of Cl^- concentration for different electrolytes.

$MgCl_2$ shows a lower free Cl^- concentration compared to the other chloride salts, due to the presence of $MgCl^+$ besides Mg^{2+}. On the other hand, all chloride salts show different Cl^- activities, especially at higher chloride concentrations. The Cl^- ions will experience a different environment and have different interactions with the counterions for the different electrolytes, which becomes more impactful at higher concentrations.[8,9] Figure S9 shows the contribution of cupric chloride species at different chloride concentrations for KCl and $CaCl_2$ electrolytes.

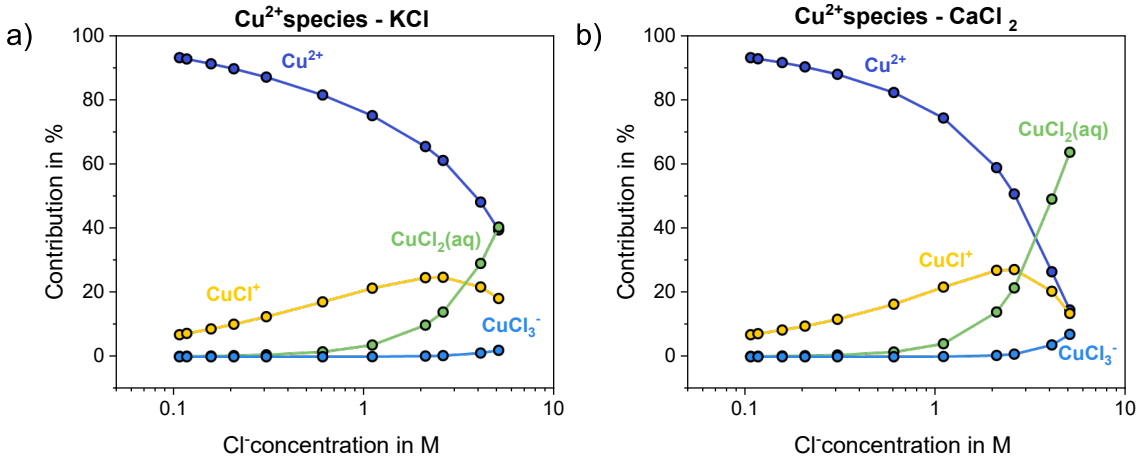

Figure S9: Copper chloride species contributions calculated by Visual Minteq. The effect of the Cl^- concentration on the Cu^{2+} chloride species for a) KCl and b) $CaCl_2$ electrolytes with 0.1 M HCl.

Similar to the cuprous chloride species contributions, Cu^{2+} will coordinate more Cl^- ligands at higher chloride concentration. In Figure S10, the same simulated solutions are presented, but this time as a function of Cl^- activity. The trends remain the same.

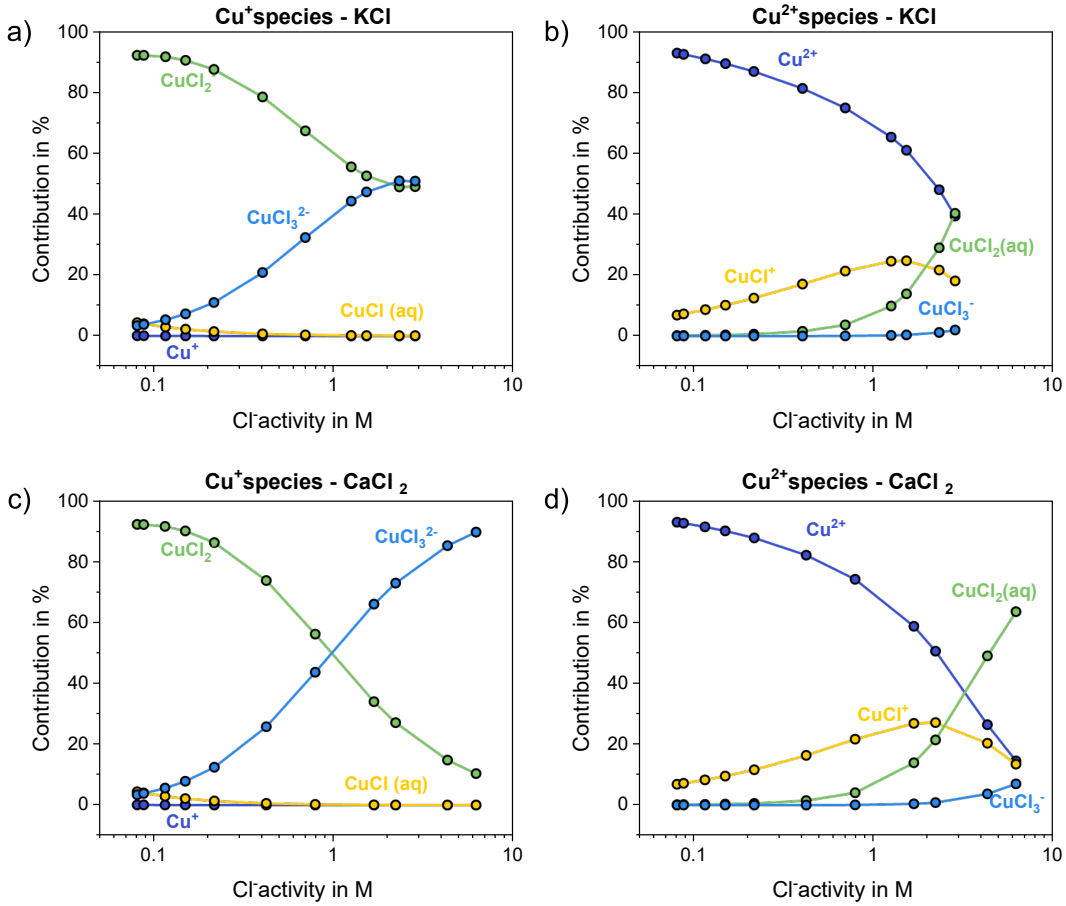

Figure S10: Copper chloride species contributions calculated by Visual Minteq as function of Cl^- activity. a) Cu^+ and b) Cu^{2+} chloride species in KCl electrolyte, and c) Cu^+ and d) Cu^{2+} chloride species in $CaCl_2$. For all the simulations, the solution consisted of 2.5 mM CuCl, 2.5 mM $CuCl_2$, 0.1M HCl and the varied electrolyte concentration.

At high chloride concentrations, the copper concentration does not affect the copper species distribution as much as the chloride concentration (Figure S11).

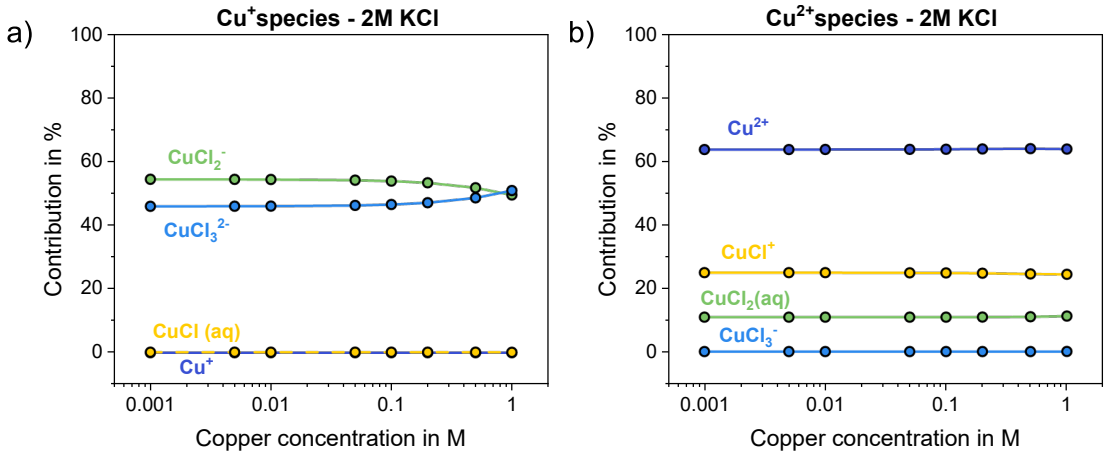

Figure S11: Copper chloride species contributions calculated by Visual Minteq as function of copper concentration for a) Cu^{+} chloride species and b) Cu^{2+} chloride species. The simulated solutions consist of 2 M KCl, 0.2 M HCl and equal amounts of CuCl and $CuCl_2$ to make up the total copper concentration.

SI-7 UV/Vis copper chlorides in KCl

UV/vis spectroscopy was performed on CuCl and $CuCl_2$ in KCl electrolytes. With increasing KCl concentration, a peak in the absorbance spectra starts to appear, for CuCl around 275 nm and for $CuCl_2$ around 250 and at 4M a broad one at 300 nm (Figure S12).

For Cu^{2+} species, absorbance below 225 nm can be assigned to Cu^{2+}, absorbance in the 240-275 nm region to $CuCl^{+}$, absorbance in the 250-300 nm region is attributed to $CuCl_2$, and absorbance in the 340-420 nm to a combination of $CuCl_3^{-}$ + $CuCl_4^{2-}$.[10] The spectra show an increase in highly coordinated Cu^{+} species with KCl concentration. The spectrum in water only shows absorbance in the Cu^{2+} region. For the KCl electrolytes, the blank shows absorbance at the lowest wavelength, making it impossible to identify the Cu^{2+} absorbance. The spectra for 0.1 M and 1.0 M KCl suggest the presence of $CuCl^{+}$ and 4.0 M KCl seems to be a combination of $CuCl^{+}$, $CuCl_2$, $CuCl_3^{-}$ and $CuCl_4^{2-}$. This is in accordance with the computational data (Figure S9).

Cu^{+} has a poor stability in air which can complicate this measurement (Figure S13). Therefore, it was important to immediately measure the sample after dissolution of CuCl (sample 1). Our spectra of CuCl, shows the appearance of a peak at 230 and 275 nm with increasing KCl concentration. These are associated with the $CuCl_2^{-}$ and $CuCl_3^{2-}$ species, respectively.[11] This is again in agreement with our computational calculations as well as literature.[11] To look at the stability of copper(I) chloride species, Figure S13 shows the spectra of CuCl over time (±10min between 1 and 3). The spectra slightly change with time, with the peak intensity of the $CuCl_2^{-}$ and $CuCl_3^{2-}$ decreasing in 1.0 M KCl and a peak at 325 nm appearing in 4.0 M KCl.

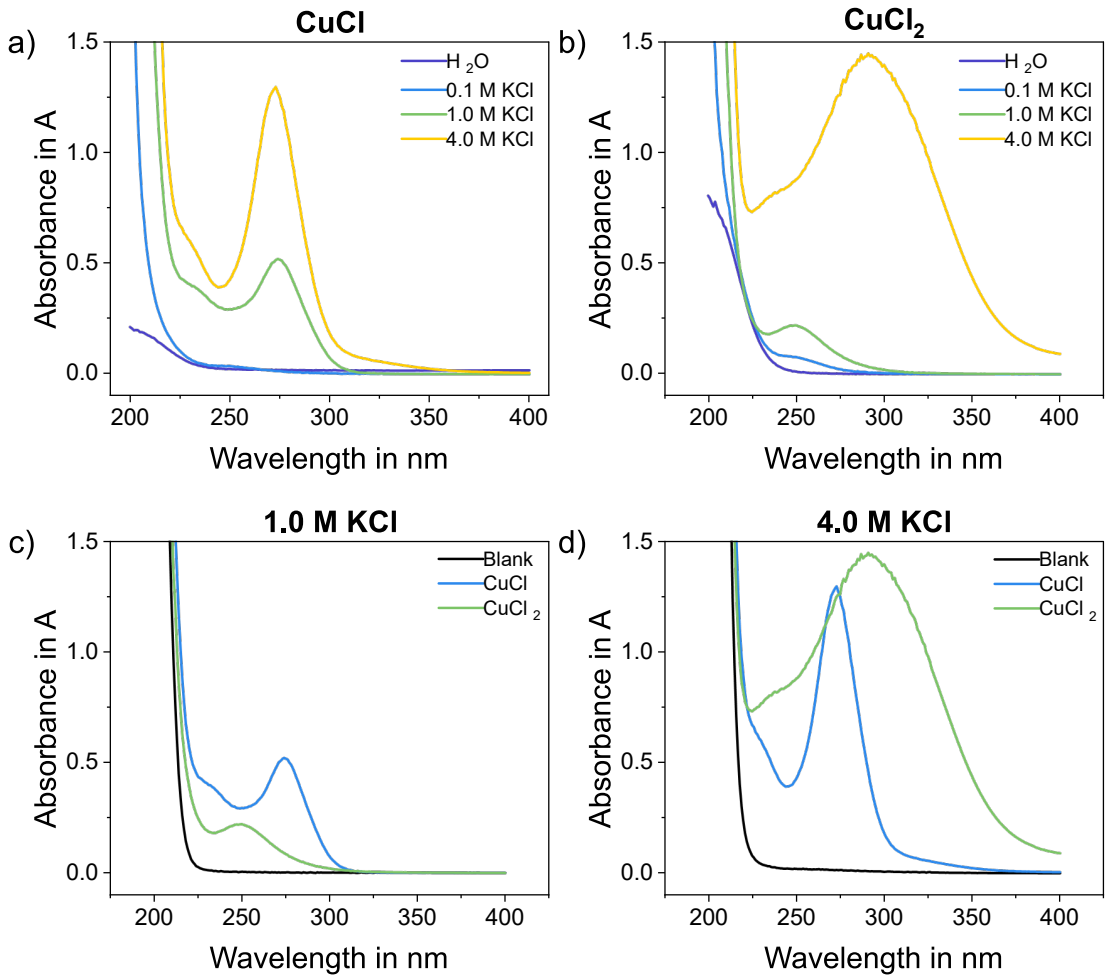

Figure S12: UV/vis spectra for a) 0.5 mM CuCl or b) 0.5 mM $CuCl_2$ in water and KCl electrolytes (0.1, 1.0, and 4.0 M). The CuCl and $CuCl_2$ spectra in c)1.0 M KCl and d) 4.0 M KCl.

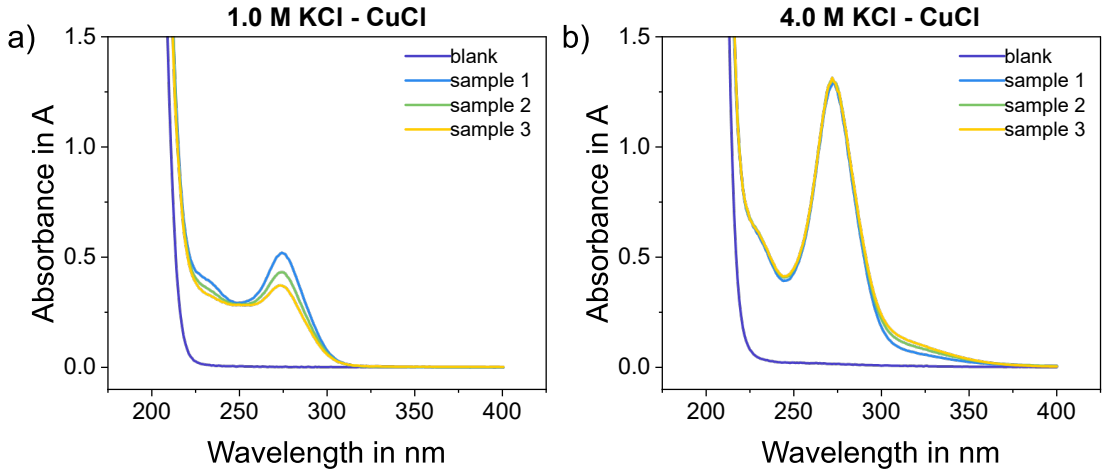

Figure S13: UV/Vis spectra of 0.5 mM CuCl in a) 1.0 M KCl and b) 4.0 M KCl. Sample 1 to 3 is from the same prepared solution, meaning sample 3 has been exposed to air for longer.

SI-8 Cyclic voltammetry copper chlorides

Figure S14 shows a couple of examples of the CV measurements for the different electrolyte solutions (1.0 M HCl, 0.5 M $MgCl_2$, 1.25 M $CaCl_2$ and 4.0 M KCl). The shapes can be very different for the different electrolytes. Notably in 1.0 M HCl, there is no clear reduction peak. Additionally, for 0.5 M $MgCl_2$ the reduction peak becomes less defined with high CO concentration. In both cases it would be difficult to read a reduction peak potential. Therefore, instead of half-wave potential shift, which requires a reduction peak potential, the oxidation peak potential shift is used for the K_{CO} determination.

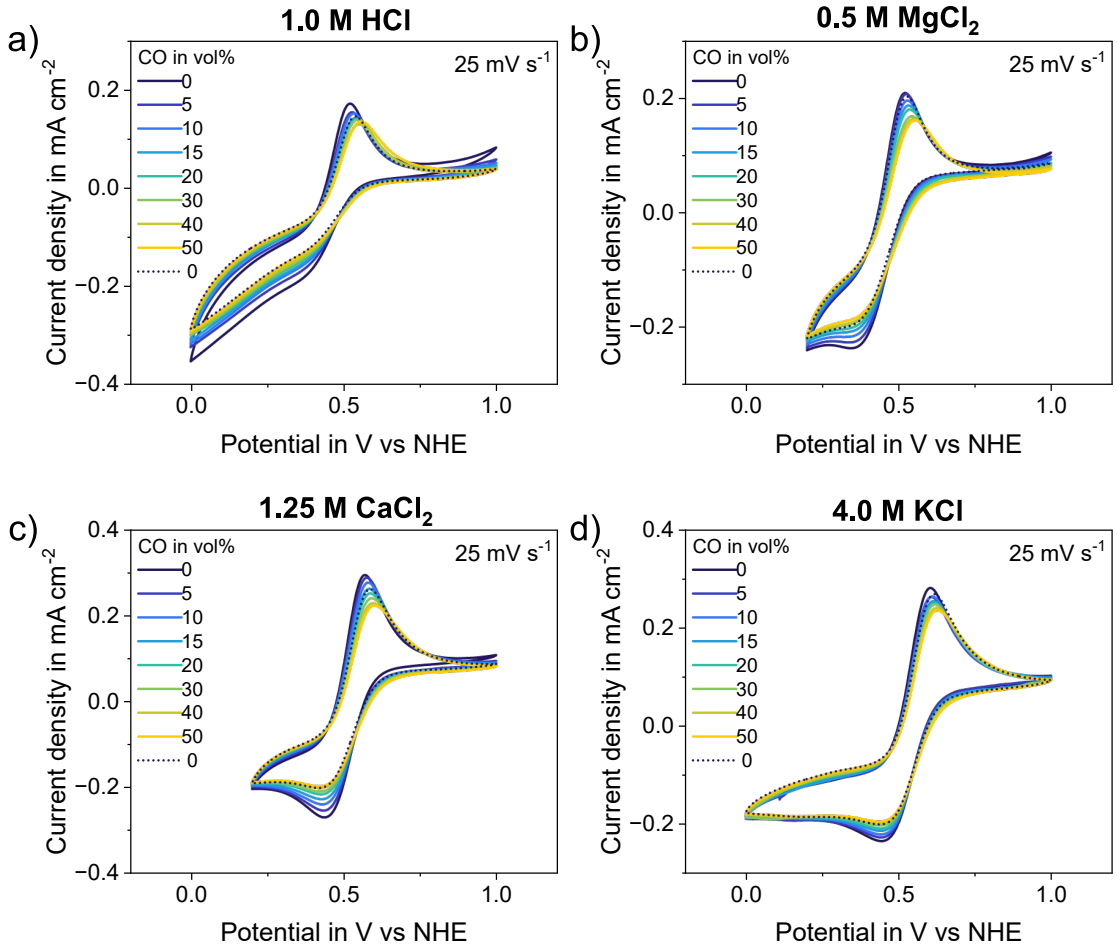

Figure S14: Examples of CV measurements for different electrolyte solutions at a scan rate of 25 mV s^{-1}. The electrolyte solutions consisted of 2.5 mM CuCl, 2.5 mM $CuCl_2$, 0.03 M HCl and a) 1.0 M HCl, b) 0.5 M $MgCl_2$, c) 1.25 M $CaCl_2$, or d) 4.0 M KCl. The gas flow rate was 2 mL min^{-1} with different CO concentrations and the remaining gas is N_2. The dotted line is the CV curve under N_2 environment after the CO curves.

Figure S14 also shows a CV curve under N_2 after the system has experienced all the CO concentrations (black dotted line). In all cases, the N_2 curve will shift back to more negative potentials, but not always completely restores to its original shape. The oxidation peak might completely return (0.5 M $MgCl_2$) or stay a bit more positive and lower in current density (1.25 M $CaCl_2$). This could be an indication of reversibility of the CO binding to the carrier. In all cases, the reduction peak seems unchanged from the last CO concentration. The decrease in reduction

current density with CO concentration and it not restoring after returning to N_2 could be because of CO adsorption on the electrode surface inhibiting the redox reaction.

SI-9 Ionic strength control experiment

To confirm the effect of Cl^- concentration independent of the total ionic strength, control experiments were performed with $CaCl_2$ and $Ca(NO_3)_2$ (Figure S15). Ideally, the salt to add has the same cation and a non-coordinating anion, to prevent other interactions of affecting the CO binding constant. Unfortunately, $Ca(ClO_4)_2$ did not seem to be compatible with our reference electrodes, leaving $Ca(NO_3)_2$ as the best option.[12,13]

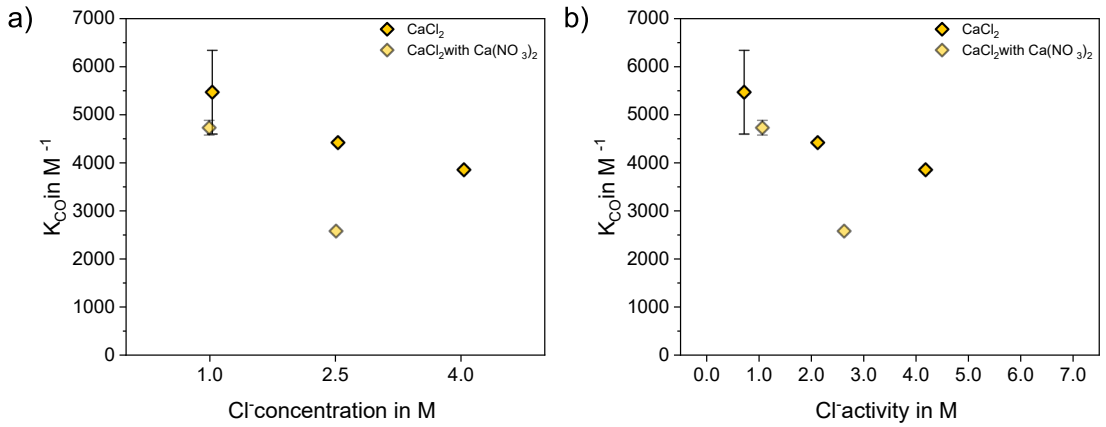

Figure S15: CO binding constant obtained from CV measurements (25 mV s^{-1}) for $CaCl_2$ electrolyte solutions plotted against a) the Cl^- concentration and b) the Cl^- activity. The faint $CaCl_2$ with $Ca(NO_3)_2$ data points represent a control where the ionic strength is kept constant at 6 M by the additions of $Ca(NO_3)_2$ salt.

Figure S15 shows a decrease in binding constant with Cl^- concentration for the two data points with the same ionic strength. Thus, the Cl^- concentration does affect the binding affinity of the copper carrier. However, the addition of $Ca(NO_3)_2$ to increase the ionic strength has also affected the binding constant as the binding constant is lower than the same $CaCl_2$ concentration without $Ca(NO_3)_2$ (Figure S15a). The binding constant at 1 M Cl^- seems to fall in line with the activity trend, but the value at 2.5 M Cl^- is a lot lower also on the activity scale (Figure S15b). Although, the NO_3^- should be weakly coordinated to copper ions, it might still affect the interactions with the copper ions.[12]

SI-10 CO binding constant with copper chloride species

To explain the differences in CO binding constant between the different electrolyte solutions we looked at the solution compositions as predicted by Visual Minteq (Figure S16).

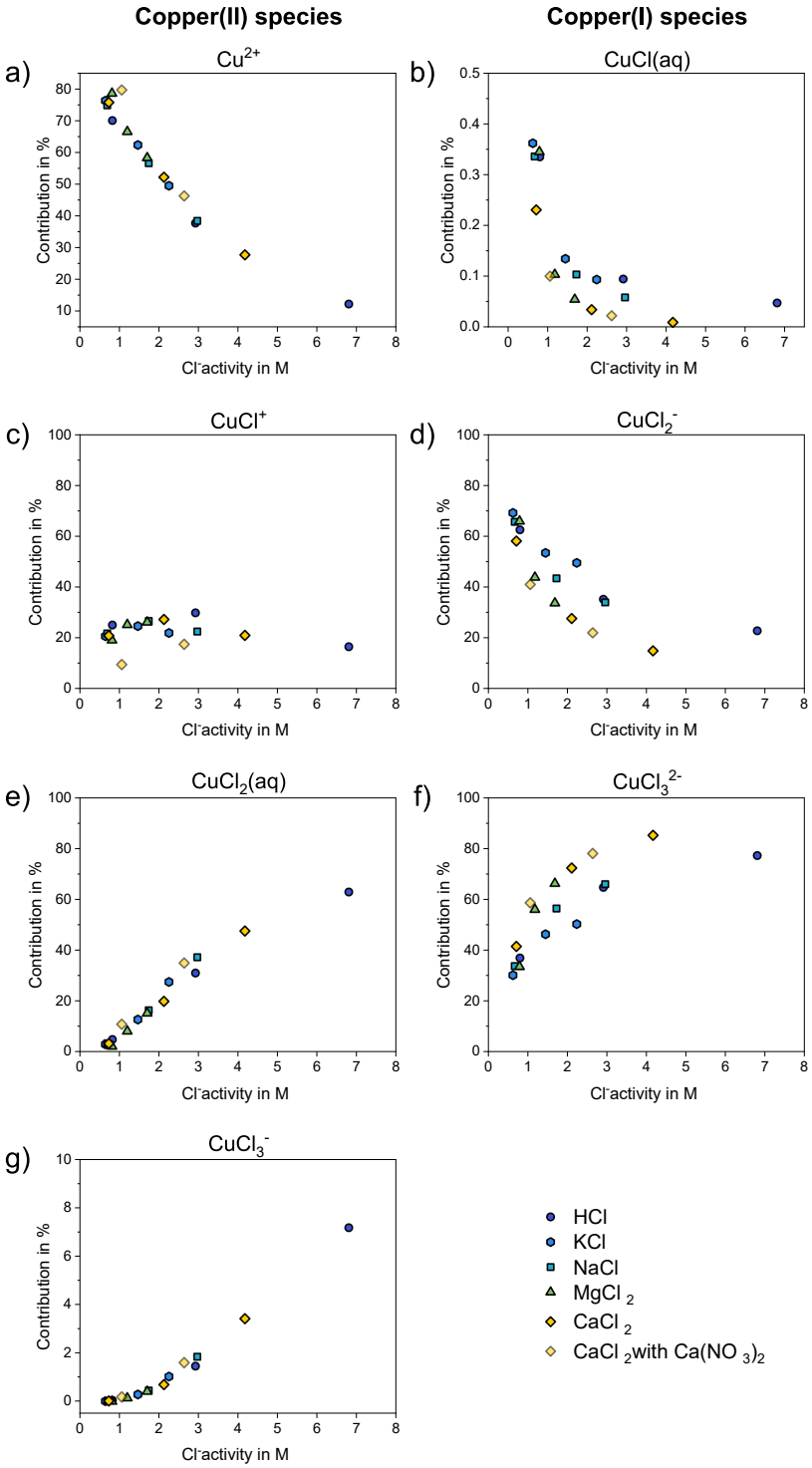

Figure S16: Copper chloride species composition of the measured electrolyte solutions calculated by Visual Minteq. a), c), e), and g) show the contribution of copper(II) species and b), d), and f) the contribution of copper(I) species to the total copper(II) and copper(I) concentration respectively.

For the different copper(II) species (Figure S16a, c, e, and g), most show a linear trend with Cl^- activity, meaning that we do not expect a different trend when plotting the K_{CO} against these species compared to the Cl^- activity. That leaves only $CuCl^+$ as a potential copper species that could explain differences between electrolytes. For the copper(I) species (Figure S16b, d and f), CuCl(aq) was shown to be the species with the strongest CO affinity making it an interesting species to search for a trend. At the same time CuCl(aq) has such a low contribution (< 0.5%) that the remaining two species together ($CuCl_2^-$ and $CuCl_3^{2-}$) make up the 100% and thus we can plot one of them to see on the x-axis to see a possible trend. We chose $CuCl_2^-$.

Figure S17 shows the K_{CO} plotted against the three species – Cu^ICl, $Cu^ICl_2^-$ and $Cu^{II}Cl^+$. However, they do not show a clear trend that explains the differences between the different electrolyte types.

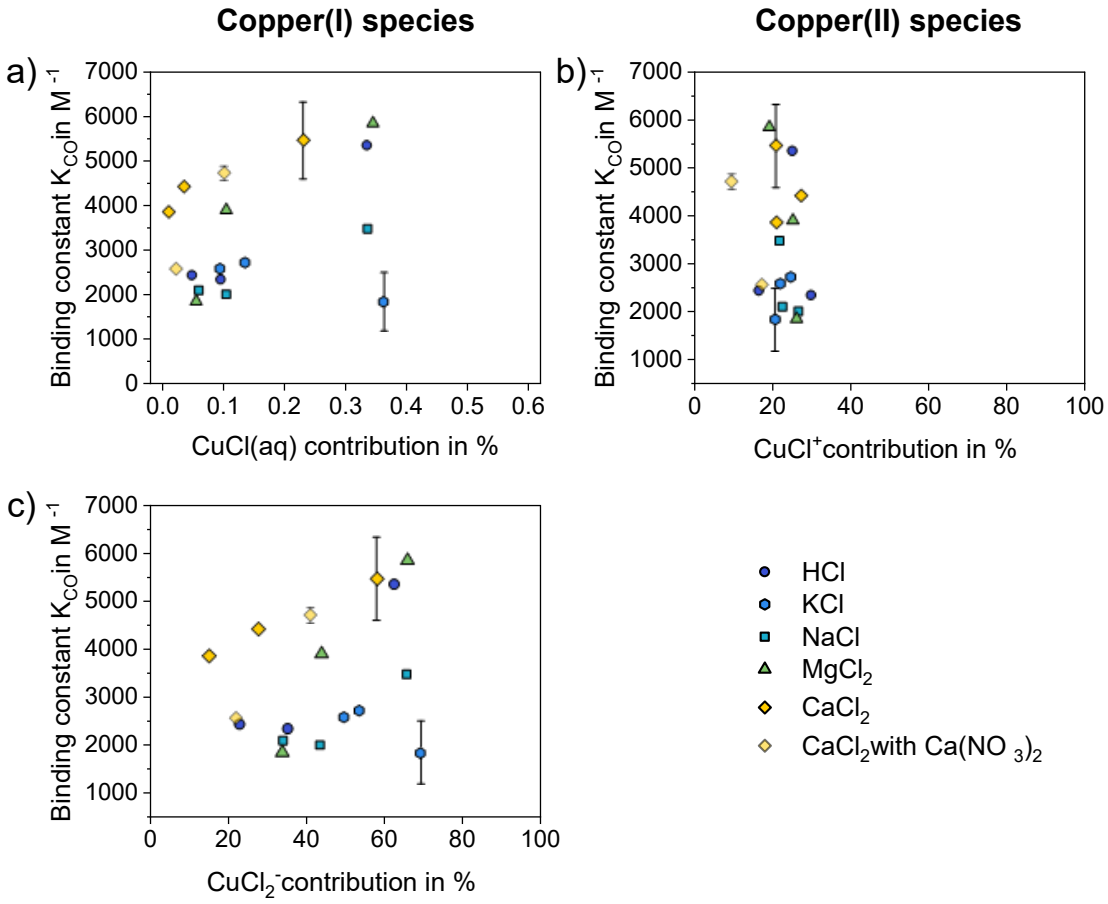

Figure S17: CO binding constant for different electrolyte solutions plotted against a) the contribution of CuCl(aq) of the Cu^+ species, b) the contribution of $CuCl_2$ of the Cu^{2+} species, and c) the contribution of $CuCl_2^-$ of the Cu^+ species for those solutions as calculated from Visual Minteq.

SI-11 CO binding at lower Cl^- concentrations

In the main text, the K_{CO} has been determined for electrolyte solutions with Cl^- concentrations of 1 M or higher. At these concentrations the copper(I) chloride species will be a mixture of $CuCl_2^-$ and $CuCl_3^{2-}$. Meng et al. show a transition of the Cu^0/Cu^+ half-wave potential at different Cl^- concentration, assigning CuCl at Cl^- concentration below 0.05 M, $CuCl_2^-$ between 0.05 M and 0.5 M and $CuCl_3^{2-}$ above 0.5 M.[4] Our experiments in the main text are all at Cl^- concentration above 0.5 M. We have also performed the same experiments at 0.1 M Cl^-, which falls in the $CuCl_2^-$ region and could still have some CuCl present according to the computational calculations (Figure 5 main text). The cyclic voltammetry measurements at different CO concentrations are presented in Figure S18.

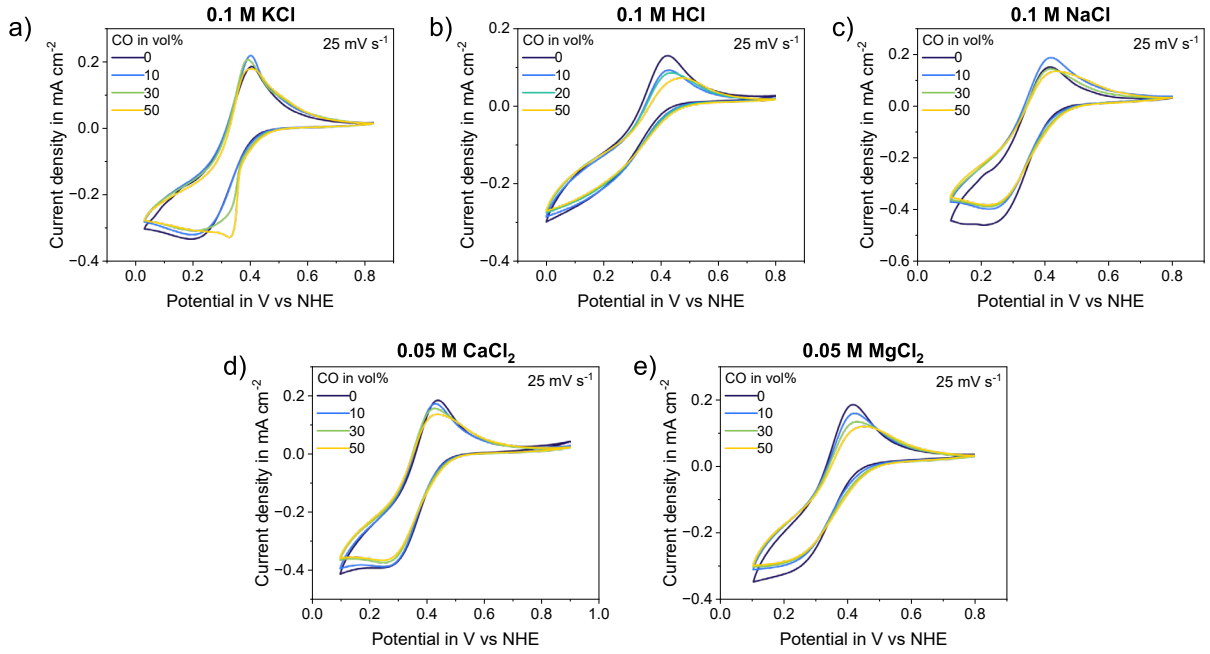

Figure S18: CV measurements for different electrolyte solutions at a scan rate of 25 mV s^{-1}. The electrolyte solutions consisted of 2.5 mM CuCl, 2.5 mM $CuCl_2$, 0.03 M HCl and a) 0.1 M KCl, b) 0.1 M HCl, c) 0.1 M NaCl, d) 0.05 M $CaCl_2$, and e) 0.05 M $MgCl_2$. The gas flow rate was 2 mL min^{-1} with different CO concentrations and the remaining gas is N_2.

Compared to the CV measurements at Cl^- concentration of 1 M or higher, the curves show a different behaviour with CO concentration. At first glance the peaks might seem to shift even stronger, which was expected with lower Cl^- concentrations. However, when trying to fit the shift with the CO partial pressure to estimate the K_{CO}, it does not give a linear line but what seems like more of an exponential increase (Figure S19).

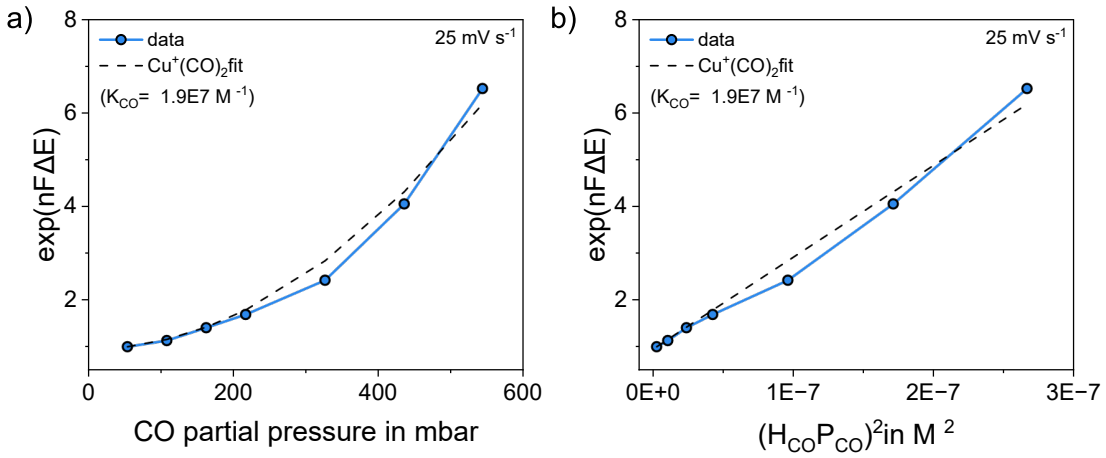

Figure S19: Fit of the potential shift with CO concentration assuming the formation of $Cu^{+}(CO)_2$ for a solution with 2.5 mM CuCl, 2.5 mM $CuCl_2$, 0.13 M HCl. The exponent of the shift is plotted against a) the CO partial pressure and b) the dissolved CO concentration to the power of 2.

As discussed in SI-3, binding of two CO ligands gives a stronger shift with partial pressure and fitting the data with the relation for $Cu^{+}(CO)_2$ gives a better fit than fitting for $Cu^{+}CO$. This would indicate the binding of two CO ligands with an overall K_{CO} of 1.9E7 M^{-1}.

However, instead of a strong shift of the redox potential, it seems that a second peak is appearing while the original peak decreases. This results in a broadening effect of the peak at high CO concentrations. Especially for 0.1 M KCl, different peaks are clearly observed when introducing CO with an additional reduction peak around 0.3 V vs NHE and an indication of an oxidation peak around 0.5 V vs NHE. The appearance of new peaks could mean the formation of strongly bound CO copper chloride complexes with their unique redox potential. Now, the shift in potential is large enough to observe the decrease in the original peak current and the appearance of a second peak, instead of it seeming like the original redox couple shifts to more positive potentials.

SI-12 CV peak shape with CO

The CV curves at low Cl^{-} concentrations seem to suggest the appearance of a second peak. This could mean that also at higher Cl^{-} concentrations a second peak appears in the presence of CO, instead of a shift of the half-wave potential. A smaller difference in standard potential with and without CO could make it appear as if the oxidation peak shifts, instead of the decrease of the original peak and increase of the new peak. Therefore, we compare the shape of the CV under N_2 and under 50 vol% CO by overlaying the two curves together with the theoretical peak shape from Bard et al.[14] To achieve this, the potentials are shifted to have the curves overlap and the currents are scaled to match peak heigh of the oxidation peak (Figure S20).

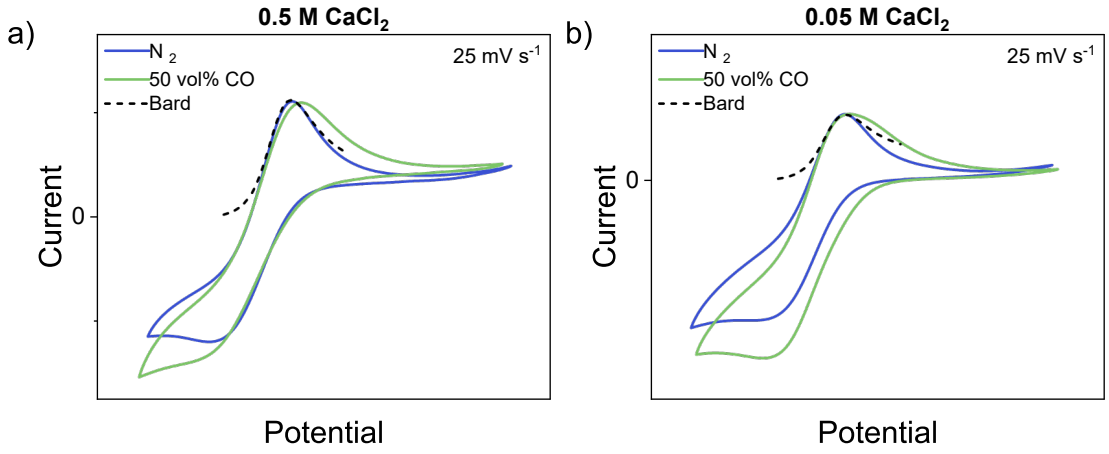

Figure S20: Overlaying of the CV curves under N_2 and 50 vol% CO environments with the Bard[14] peak shape curve for a) 0.5 M $CaCl_2$ and b) 0.05 M $CaCl_2$. The total copper concentration is 5 mM ($CuCl/CuCl_2$) and the scan rate is 25 mV s^{-1}. The curves are shifted on the potential scale and the current is scaled to overlay the curves for shape comparison.

In both cases, the CV curve under N_2 shows better agreement with the theoretical peak shape from Bard, compared to the CV curve under CO. Figure S20a shows a broadening of the oxidation peak under 50 vol% CO for 0.5 M $CaCl_2$, which supports that this could be two peaks overlapping, instead. This is similar to the clear peak broadening effect that we saw for the low chloride concentrations (Figure S20b, 0.05 M $CaCl_2$). This could have implications for the method to determine the K_{CO} from the potential shift. Previously, we determined the binding constant from the contributions of two peaks to the total curve.[15] However, this requires a larger separation between the unbound and CO-bound carrier peaks to be able to identify and fit the CO-carrier peak. For this work, where the two peaks overlay and are not distinguishable, we believe the potential shift with CO concentration still offers a good approximation of the binding constant as a stronger binding will result in a seemingly bigger shift of the overlayed peaks. Similarly to the different redox potentials of the different copper chloride species, the observed redox peak will be a weighted average of the different redox species.[16] Thus, a higher binding constant will result in a larger contribution of the CO-bound curve and appear as a stronger shift of the curve to more positive potentials.

SI-13 Electrolyte solution Figure 8c and d

Table S2 presents the composition, pH and conductivity of the electrolyte solutions measured for the Cu^+ stability at different $Cu:Cl^-$ ratios as presented in Figure 8c and d.

Table S2: Composition, pH and conductivity for the solutions tested in Figure 8c and d.

Cu:Cl^-	K_2SO_4 in M	KCl in M	$CuSO_4$ in mM	pH	Conductivity in mS cm^{-1}
1:0	0.5	0	10	5.49	87.5
5:1	0.4988	0.002	10	5.37	97.2
1:1	0.4938	0.01	10	5.16	97.6
1:2	0.4875	0.02	10	4.32	97.9
1:5	0.4688	0.05	10	5.05	96.9
1:10	0.4375	0.1	10	5.41	98.0
1:50	0.1875	0.5	10	5.07	100.5
1:80	0	0.8	10	5.05	92.4

SI-14 Cu^+ stability as a function of Cl^- concentration and Cl^-/Cu ratio

The half-wave potentials of the Cu^0/Cu^+ and Cu^+/Cu^{2+} redox couples at different Cl^- concentrations and Cl^-/Cu ratios are presented in Figure S21. The data points connected by line all have the same total copper concentration of 10 mM, while the separate data points at around 4 M have a total copper concentration of 100 mM, resulting in a ten times lower Cl^-/Cu ratio. The increase in copper concentration does not affect the Cu^+/Cu^{2+} redox potential, but the Cu^0/Cu^+ shifts to slightly more positive potentials. Thus, the smaller Cl^-/Cu ratio (42) decreases the stability window of Cu^+ but is larger than the stability window of higher Cl^-/Cu ratios (105) at lower absolute Cl^- concentrations. Therefore, the absolute Cl^- concentration seems to be determining over the Cl^-/Cu ratio.

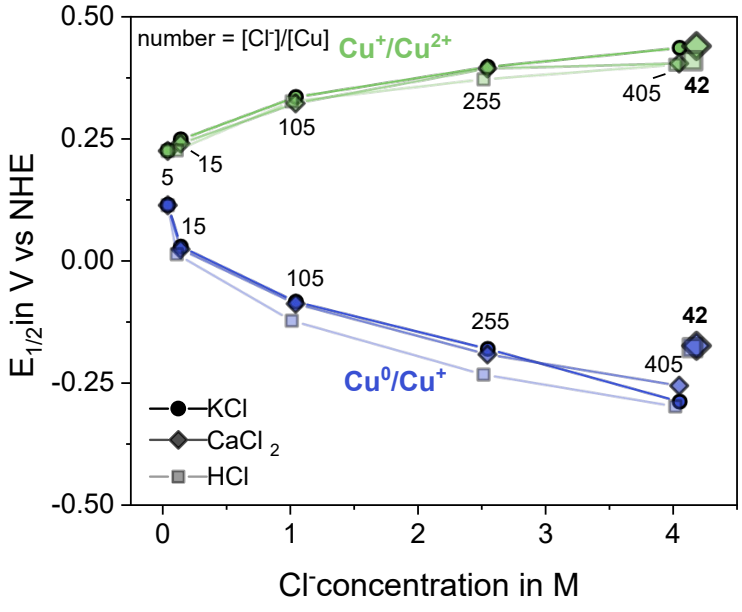

Figure S21: Half-wave potential of the Cu^0/Cu^+ and Cu^+/Cu^{2+} reactions at the different Cl^- concentrations for KCl, $CaCl_2$ and HCl electrolytes. The numbers indicate the ratio of Cl^- over Cu, with the separate data points at 4.2 M Cl^- having increased copper concentration to have a smaller Cl^-/Cu ratio at a high absolute Cl^- concentration. The solutions consist of 5 mM CuCl, 5 mM $CuCl_2$, 0.03M HCl, and the electrolyte at the different Cl^- concentrations (0, 0.1, 1.0, 2.5 and 4M). The separate data points are from a solution of 50 mM CuCl, 50 mM $CuCl_2$, 0.03M HCl, and 2 M $CaCl_2$ or 4 M HCl.

SI-15 Effect of HCl concentration on reversibility of CV

With HCl concentration from 0.001 M to 1.0 M the Cu^{+}/Cu^{2+} reversibility decreases, resulting in the disappearance of the reduction peak (Figure S22a). In this case the total Cl^{-} is kept the same by having a mixture of KCl and HCl (Table S3). Interestingly, increasing the HCl concentration from 1.0 M tot 4.0 M, the reversibility of the Cu^{+}/Cu^{2+} redox couple returns (Figure S22b). Here, the total Cl^{-} concentration varies as no KCl is added to compensate.

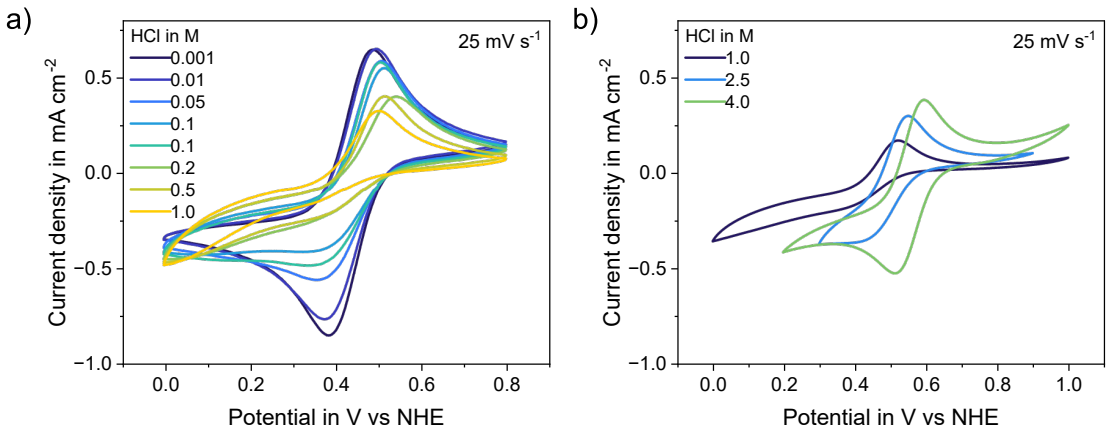

Figure S22: Effect of HCl concentration on the Cu^{+}/Cu^{2+} redox couple. a) Constant chloride concentration (1 M) with variable HCl concentration through mixtures of HCl and KCl electrolyte and 10 mM $CuCl_2$. b) Electrolyte solutions from K_{CO} measurements with 5 mM CuCl/$CuCl_2$.

The non-reversible character of the Cu^{+}/Cu^{2+} complex at 1 M HCl solutions, make it less suitable as electro-active carrier, where switchability between Cu^{+} and Cu^{2+} is important for the capture and release of CO.

Table S3: Composition, pH and conductivity for the solutions tested in Figure S22a.

Solution	HCl in M	KCl in M	$CuCl_2$ in mM	pH	Conductivity in mS cm^{-1}
1	0	1	10	4.05	124.2
2	0.001	0.999	10	3.39	124.7
3	0.01	0.99	10	2.30	124.8
4	0.05	0.95	10	1.73	125.8
5	0.1	0.9	10	1.43	127.9
6	0.2	0.8	10	1.10	130.5
7	0.5	0.5	10	0.77	139.5
8	1	0	10	0.51	159.9

SI-16 CO capture and release experiments

Table S4 shows the capture results of Method 2, where the applied potential is relative to the open circuit potential of the carrier solutions at equimolar amounts of Cu^{+} and Cu^{2+}.

Table S4: CV determined and experimental values for CO capacity and carrier utilisation of a 20 mM copper chloride solution. Method 2 uses the same change in potential from the measured OCP (OCP – 0.35 V for reduction).

		1.0 M KCl	**1.0 M HCl**	**0.5 M $CaCl_2$**
CV determined	K_{CO} (M^{-1})	1850	5350	5500
	CO capacity (mL)	1.2	2.9	3.0
	Cu utilisation (%)	9	22	22
Method 2	CO capacity (mL)	1.30	1.44	1.49
	Cu utilisation (%)	9.7	10.7	11.1

The effect of copper concentration on the copper species

The CV measurements to determine the K_{CO} are performed in the electrolyte solution with 5 mM of copper ions, while the absorption experiments are performed in the same electrolyte solution but with 20 mM of copper ions. If the copper concentration affects the copper species contributions, it could also affect the binding constant of the carrier solution. Table S5 presents the copper species distribution in the electrolyte solutions for the CV measurement and the absorption measurements, calculated by Visual Minteq.

Table S5: Copper species distribution in % for the electrolyte solutions at the different copper ion concentrations (5 and 20 mM) used for the CV measurement and absorption measurement, respectively. The values are calculated by Visual Minteq

		Copper(I) species in %				**Copper(II) species in %**		
	Cu in mM	**Cu^{+}**	**CuCl (aq)**	**$CuCl_2^{-}$**	**$CuCl_3^{2-}$**	**Cu^{2+}**	**$CuCl^{+}$**	**$CuCl_2$(aq)**
1.0 M KCl	5	0.00	0.33	67.3	32.3	75.0	21.4	3.6
	20	0.00	0.33	67.1	52.6	75.0	21.3	3.6
1.0 M HCl	5	0.00	0.24	50.4	49.3	74.2	21.7	4.1
	20	0.00	0.24	50.2	49.5	74.2	21.7	4.1
0.5 M $CaCl_2$	5	0.00	0.3	59.9	39.8	68.0	25.9	6.0
	20	0.00	0.31	60.3	39.4	68.5	25.7	5.8

The estimated copper species distribution shows no significant difference between the solutions with 5 mM copper ions or 20 mM copper ions. Therefore, it is not expected to have different binding constants for the carrier solution used for the CV measurements than the carrier solution used for the absorption measurements.

Number of CO ligands per carrier

The deviation from the predicted capture capacity based on the K_{CO}, could be caused by a different number of CO ligand per carrier than one. Although, our CV experiments showed the best fit for one CO ligand (Figure S5). If we look at the different complexes, $(Cu^+)_2CO$, Cu^+CO, and $Cu^+(CO)_2$, the estimated binding constant would predict the CO/carrier ratio presented in Figure S23.

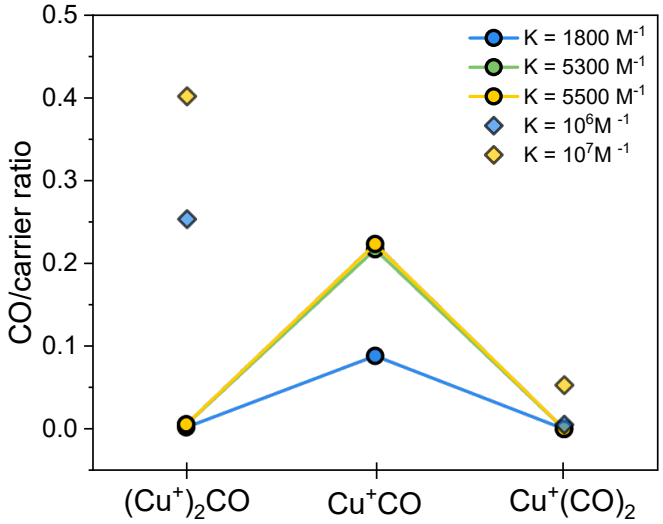

Figure S23: Theoretical CO/carrier ratio based on the estimated K_{CO} for 1 M KCl (1800 M^{-1}), 1 M HCl (5300 M^{-1}), and 0.5 M $CaCl_2$ (5500 M^{-1}) for the different number of CO ligands per copper. For a bridging ligand $(Cu^+)_2CO$ or 2 terminal CO ligands $Cu^+(CO)_2$, the K_{CO} would be estimated to be 10^6 M^{-1} for 1 M KCl and 10^7 for 0.5 M $CaCl_2$ and are represented in the single datapoints.

$(Cu^+)_2CO$ with the adjusted K_{CO} for this carrier-CO interaction (10^6 or 10^7 M^{-1}, SI-3) does not explain the deviation in our experimental results. Although the relative effect of the binding constant for $(Cu^+)_2CO$ should be smaller compared to Cu^+CO (CO_{CaCl2}/CO_{KCl} =1.6 vs CO_{CaCl2}/CO_{KCl} =2.5), the expected CO capacity is higher than for Cu^+CO and higher than our experimental results. $Cu^+(CO)_2$ shows the opposite trend – the expected CO capacity is lower (but too low), and the relative effect of the binding constant is larger (CO_{CaCl2}/CO_{KCl} = 9.8). Together with the CV experiments, Cu^+CO still seems the most likely complex during CO capture.

References

1 Oschatz, M. & Antonietti, M. A search for selectivity to enable CO2 capture with porous adsorbents. *Energy & Environmental Science* **11**, 57–70 (2018). https://doi.org/10.1039/C7EE02110K

2 Gagne, R. R., Allison, J. L. & Ingle, D. M. Unusual structural and reactivity types for copper(I). Equilibrium constants for the binding of monodentate ligands to several four-coordinate copper(I) complexes. *Inorganic Chemistry* **19**, 2767–2774 (1979).

3 Addison, A. W., Carpenter, M., Lau, L. K.-M. & Wicholas, M. Coordination Sphere Flexibility at Copper: Chemistry of a Unipositive Copper(II) Macrocycle, [Cu(cyclops)]$^{+}$. *Inorganic Chemistry* **17**, 1545–1552 (1978).

4 Meng, Y. & Bard, A. J. Measurement of Temperature-Dependent Stability Constants of Cu(I) and Cu(II) Chloride Complexes by Voltammetry at a Pt Ultramicroelectrode. *Analytical Chemistry* **87**, 3498–3504 (2015). https://doi.org/10.1021/acs.analchem.5b00052

5 Heyrovsky, J. & Kuta, J. *Principles of Polarography*. (Academic Press, 1965).

6 Goldman, A. S. & Krogh-Jespersen, K. Why Do Cationic Carbon Monoxide Complexes Have High C−O Stretching Force Constants and Short C−O Bonds? Electrostatic Effects, Not σ-Bonding. *Journal of the American Chemical Society* **118**, 12159–12166 (1996). https://doi.org/10.1021/ja960876z

7 Yi, H.-B., Xia, F.-F., Zhou, Q. & Zeng, D. [CuCl3]− and [CuCl4]2− Hydrates in Concentrated Aqueous Solution: A Density Functional Theory and ab Initio Study. *The Journal of Physical Chemistry A* **115**, 4416–4426 (2011). https://doi.org/10.1021/jp109723v

8 Khoshkbarchi, M. K. & Vera, J. H. Measurement and correlation of ion activity in aqueous single electrolyte solutions. *AIChE Journal* **42**, 249–258 (1996). https://doi.org/https://doi.org/10.1002/aic.690420121

9 Wilczek-Vera, G., Rodil, E. & Vera, J. H. On the activity of ions and the junction potential: Revised values for all data. *AIChE Journal* **50**, 445–462 (2004). https://doi.org/https://doi.org/10.1002/aic.10039

10 Lacarbonara, G., Albanelli, N., Fazzi, D. & Arbizzani, C. A spectroelectrochemical study of copper chloro-complexes for high performance all-copper redox flow batteries. *Electrochimica Acta* **458**, 142514 (2023). https://doi.org/https://doi.org/10.1016/j.electacta.2023.142514

11 Horváth, O. & Papp, S. Photo-oxidation of copper(I) chloro complexes: Individual quantum yields of [CuCl2]− and [CuCl2]−2. *Journal of Photochemistry* **30**, 47–61 (1985). https://doi.org/https://doi.org/10.1016/0047-2670(85)87005-2

12 Keškić, T. *et al*. What Is the Nature of Interactions of BF4−, NO3−, and ClO4− to Cu(II) Complexes with Girard's T Hydrazine? When Can Binuclear Complexes Be Formed? *Crystal Growth & Design* **19**, 4810–4821 (2019). https://doi.org/10.1021/acs.cgd.9b00760

13 Mondal, A., Reddy, K. P., Som, S., Chopra, D. & Kundu, S. Nitrate and Nitrite Reductions at Copper(II) Sites: Role of Noncovalent Interactions from Second-Coordination-Sphere. *Inorganic Chemistry* **61**, 20337–20345 (2022). https://doi.org/10.1021/acs.inorgchem.2c02775

14 Bard, A. J. & Faulkner, L. R. *Electrochemical Methods Fundamentals and Applications*. (John Wiley & Sons, 2001).

15 Koopman, C. I., Albertsma, J., van der Veen, M. A. & Vermaas, D. A. Electrochemically Mediated Separation of Carbon Monoxide Using a Ni-Based Redox Couple. *ACS Energy Letters* (2026). https://doi.org/10.1021/acsenergylett.5c04138

16 Zhao, H., Chang, J., Boika, A. & Bard, A. J. Electrochemistry of High Concentration Copper Chloride Complexes. *Analytical Chemistry* **85**, 7696–7703 (2013). https://doi.org/10.1021/ac4016769